Enhancing Open-Circuit Voltage of High-Efficiency Non-Fullerene Ternary Solar Cells with a Star-Shaped Acceptor

Guilong Cai,*[,†,‖] Yuhao Li,[†,‖] Jiadong Zhou,[§] Peiyao Xue,[‡] Kuan Liu,[⊥] Jiayu Wang,[‡] Zengqi Xie,[§] Gang Li,[⊥] Xiaowei Zhan[‡] and Xinhui Lu*[,†]

[†] Department of Physics, The Chinese University of Hong Kong, New Territories 999077, Hong Kong, China

[‡] Department of Materials Science and Engineering, College of Engineering, Key Laboratory of Polymer Chemistry and Physics of Ministry of Education, Peking University, Beijing 100871, China

[§] State Key Laboratory of Luminescent Materials and Devices, South China University of Technology, Guangzhou 510640, China

[⊥] The Department of Electronic and Information Engineering, Research Institute for Smart Energy (RISE), The Hong Kong Polytechnic University, Hung Hom, Kowloon 999077, Hong Kong, China

[‖] Contributed equally

ABSTRACT:

Ternary strategy has been widely used in high-efficiency organic solar cells (OSCs). Herein, we successfully incorporated a mid-bandgap star-shaped acceptor, FBTIC as the third component into the PM6/Y6 binary blend film, which not only achieved a panchromatic absorption, but also significantly improved the open-circuit voltage (V_{OC}) of the devices due to the high-lying lowest unoccupied molecular orbital (LUMO) of the FBTIC. Morphology characterizations show that star-shaped FBTIC molecules are amorphously distributed in the ternary system, and the finely tuned ternary film morphology facilitates the exciton dissociation and charge collection in ternary devices. As a result, the best PM6/Y6/FBTIC-based ternary OSCs achieved a power conversion efficiency (PCE) of 16.7% at a weight ratio of 1.0/1.0/0.2.

KEYWORDS: star-shaped acceptor, non-fullerene acceptor, organic solar cell, fused-ring electron acceptor, ternary

1. INTRODUCTION

Organic solar cells (OSCs) based on the bulk heterojunction (BHJ) device structure have many potential advantages over conventional silicon-based solar cells, such as solution processability, roll-to-roll fabrication, low cost, light weight, mechanical flexibility and semitransparency, and are therefore of great interest to solar cell research community.[1-4] Conventional fullerene derivative based electron acceptors exhibit intrinsic disadvantages, such as poor absorption in the near-infrared (NIR) region, limited electronical tunability, poor photostability and thermal stability.[5-9] In 2015, a kind of new non-fullerene electron acceptor - "fused-ring electron acceptor (FREA)" was invented by Zhan's group and tremendously boosted the research in OSCs.[10, 11] Generally, the crystallinity, absorption and energy levels of FREAs can be tuned by the chemical tailoring of fused-ring core,[12-32] end groups[33-44] and side chains[45-50] to regulate the morphology of active layer films and to improve the optical and electrical properties of OSCs. The power conversion efficiencies (PCE) of OSCs based on FREAs has reached 17%, largely surpassing those of fullerene-based OSCs.[51-55]

Recently, a low-bandgap non-fullerene electron acceptor, 6,11-bis(5,6-difluoro-3-(dicyanomethylene)-2*Z*-methylene-indan-1-one)-8,9-bis(2-ethylhexyl)-5,12-diundecyl-8,9-dihydro-bis(thieno[2',3':4,5]thieno[3,2-*b*]pyrrolo)[3',2':3,4;2",3":5,6]benzo[1,2-*c*][1,2,5]thiadiazole (Y6), has been reported by Yuan et al.[56] Through combining with a mid-bandgap polymer donor poly(4,8-bis(5-(2-ethylhexyl)-4-fluorothiophen-2-yl)benzo[1,2-b:4,5-*b*']dithiophene-2,6-diyl)-*alt*-(5,5'-(5,7-bis(2-ethylhexyl)benzo[1,2-*c*:4,5-*c*']dithiophene-4,8-dione-1,3-diyl)bis(thiophen-2-yl)) (PM6), the PM6/Y6-based

OSCs exhibit high PCEs of 15-16%, with a broad and strong photo-absorption in the 500-900 nm spectral region and a low energy loss of 0.5-0.6 eV. However, there still exist some shortcomings in Y6, including the relatively poor light absorption in the range of 650-750 nm; and interrupted π-conjugation based on the crystallographic analysis,[57] which might prevent the electron transport in the homogeneous domain and induce large non-radiative recombination. At the same time, a mid-bandgap star-shaped FREA, 2,7,12-tris(5,6-difluoro-3-(dicyanomethylene)-2*Z*-methylene-indan-1-one)-4,4,9,9,14, 14-hexakis(4-hexylphenyl)-4,9,14-trihydro-benzo[1,2-*b*:3,4-*b*':5,6-*b*"]tri(cyclopenta [1,2-*b*:5,4-*b*']dithiophene) (FBTIC),[15] was synthesized and reported by our group. Specially, FBTIC exhibits intense light absorption in 650-750 nm and higher electron charge mobility (1.7×10^{-3} cm^2 V^{-1} s^{-1}).

Introducing a proper third component to fabricate ternary OSCs is an effective and low-cost strategy to improve the device performance. The fabrication of the first ternary BHJ OSC dates back to 2005. Thompson et al. added PPV polymer as a third component to the binary system, which effectively extended the range of light absorption to absorb low-energy photons.[58] The third component applied in benchmark devices can be polymer donors,[59] small molecule donors,[60, 61] fullerene acceptors,[62, 63] and non-fullerene acceptors.[64-69] Ternary cells offer noticeable advantages over binary cells, such as, extending the absorption and improving overall light harvesting, being beneficial to the short-current current density (J_{SC}); reducing the energy loss and thus enhancing the device open-circuit voltage (V_{OC}). Moreover, it can utilize excellent optical, electrical and morphological properties of high-performance acceptors, such as

Y6, while flexibly regulating film morphology to improve the exciton dissociation, charge transfer and thus fill factor (FF). To date, most of the acceptors employed as the third component have linear-shaped chemical structures. The utilization of star-shaped acceptors with 3D stacking has not been explored in ternary devices.[70-72]

In this study, star-shaped FBTIC was added to the PM6/Y6 binary device as the third component in order to improve the performance. The light absorption of FBTIC is complementary to the absorption of the PM6/Y6 binary film. Furthermore, FBTIC and Y6 form non-radiative fluorescence resonance energy transfer, further contributing to the light harvesting. In addition, the intermolecular π-π stacking of FBTIC leads to complex three-dimensional (3D) conjugated framework as suggested by the single crystal analysis, and multichannel charge transport based on 3D conjugated framework is beneficial for the FF improvement. Owing to above advantages, the optimized ternary OSCs based on PM6/Y6/FBTIC exhibited improved V_{OC} and FF compared with the binary counterparts, achieving a high PCE of 16.7%.

2. RESULTS AND DISCUSSION

2.1. Chemical Structure and Characterization

Figure 1 displays the chemical structures of FBTIC, Y6 and PM6. FBTIC is synthesized according to our previously published procedures.[15] In addition, Y6 demonstrates dual and arched conformation while FBTIC demonstrates the triad and star-shaped conformation.

The FREAs are always in acceptor-donor-acceptor (A-D-A) or A-D-A'-D-A type, and the arrangement of D-A fragment is of importance for tuning molecular stacking,

spectral absorption and energy level. Similar to the polycondensation, D-A fragment could be regarded as the pendent functionality to form the conjugated framework by head-to-head/tail stacking. As suggested by signal crystal analysis, depending on the number of functional groups, Y6 tends to form the one-dimensional wavy intermolecular chain and FBTIC tends to form crosslinked motif as illustrated in Figure 2. Although the chains are packed by H-bonding linking in Y6 crystallite, the π-conjugation is interrupted, which prevents the electron transport in the homogeneous domain.[57, 73] The additional FBTIC could serve as cross-linking functionality to construct the 3D conjugated framework, which provide the multichannel electron transport.[15]

The absorption peaks of PM6, FBTIC and Y6 solid film are located at 618, 705 and 835 nm, respectively (Figure 3a), and this combination of materials achieves a panchromatic absorption. In addition, the lowest unoccupied molecular orbital (LUMO) energy level of Y6 is −4.10 eV, while FBTIC, on the other hand, has an up-shifted LUMO of −3.85 eV, which can improve the V_{OC} of the ternary OSCs because the V_{OC} is definitely related to the difference between the LUMO of the acceptor and the highest occupied molecular orbital (HOMO) of the donor (Figure 3b).

2.2. Photovoltaic Cells

The BHJ OSCs were fabricated in a conventional device configuration of indium tin oxide (ITO) glass/PEDOT:PSS/active layer/PNDIT-F3N/Ag. The V_{OC}, J_{SC}, FF and PCE of the binary and ternary OSCs with different D/A weight ratios are summarized in Table 1. For both binary and ternary OSCs, the weight ratio of the polymer donor to

the acceptor(s) is chosen to be 1/1.2 containing 0.5% (v/v) chloronaphthalene (CN). In addition, the current density–voltage (*J*–*V*) curves of the optimal binary and ternary OSCs are exemplified in Figure 4a and Figure S1a. The best PCE of optimized Y6-based binary device is 16.0% with a V_{OC} of 0.841 V, a J_{SC} of 24.7 mA cm^{-2}, and a FF of 77.3%, while the best PCE of optimized FBTIC-based binary device is 8.84% with a V_{OC} of 0.908 V, a J_{SC} of 14.6 mA cm^{-2} and a FF of 66.6%. Then, ternary OSCs were fabricated based on different concentrations of FBTIC. With the gradually increase of FBTIC, the V_{OC} of the ternary device is improved due to the higher LUMO energy level of FBTIC compared to that of Y6, while the J_{SC} of the ternary devices is improved first and reduced then. In particular, the ternary cell exhibits a champion PCE of 16.7% with a V_{OC} of 0.866 V, a J_{SC} of 24.6 mA cm^{-2} and a FF of 77.9% when the weight ratio of PM6/Y6/FBTIC is 1.0/1.0/0.2, whereas the PCEs are 16.5% and 15.8% when the corresponding ratios are 1.0/1.1/0.1 and 1.0/0.9/0.3, respectively. In addition, The inverted device with a configuration of ITO/ZnO/PM6:Y6:FBTIC(1.0/1.0/0.2)/MoO_3/Ag exhibited a relatively lower PCE of 14.5% (Table 1 and Figure S1). Therefore, the appropriate proportion of star-shaped blue-shifted FBTIC as a third component can effectively increase the V_{OC} and FF without significantly sacrificing the high J_{SC} of the PM6/Y6 binary system.

The external quantum efficiencies (EQE) of the best OSCs of PM6/Y6, PM6/FBTIC and PM6/Y6/FBTIC (1.0/1.0/0.2) were measured and displayed in Figure 4b and S1b. Devices of PM6/Y6 and PM6/Y6/FBTIC show similar EQE spectra between 300 and 930 nm. The J_{SC} of the best devices based on EQE are consistent with

the J_{SC} of the corresponding devices obtained from J-V curves (<5% mismatch, Table 1).

In order to study the exciton dissociation and charge collection of the optimal binary and ternary devices, the relationship between the photocurrent density (J_{ph}) and the effective voltage (V_{eff}) of the cells was investigated (Figure 4c and Table S1). The exciton dissociation efficiency (η_{diss}) and the charge collection efficiency (η_{coll}) can be calculated by the ratio of J_{ph} and the saturation photocurrent density (J_{sat}) under the short circuit condition and the maximal power output condition, respectively.[74, 75] The η_{diss} of optimal PM6/Y6, PM6/FBTIC and PM6/Y6/FBTIC (1.0/1.0/0.2) devices are 92.8%, 88.0% and 94.6%, and the same trend applies to η_{coll}. Obviously, the ternary devices containing an appropriate proportion of FBTIC will effectively increase the exciton dissociation and the charge collection efficiency compared to the binary OSCs.

The space charge limited current (SCLC) measurement[76, 77] was used to measure the mobilities of the binary and ternary active layers (Figure S2). Compared to the PM6/FBTIC, the active layers of PM6/Y6 and PM6/Y6/FBDIC (1.0/1.0/0.2) exhibit slightly higher hole mobility (μ_h), electron mobility (μ_e) and μ_h/μ_e (Table S2), which contribute to the improvement of FF. And ternary blend OSC exhibits the most balanced charge mobility, in consistent with its highest FF.

The photoluminescence (PL) measurement was used to obtain the information of intermolecular interactions between Y6 and FBTIC (Figure 4d). Compared to the neat Y6 and Y6/FBTIC (1.0/0.2) blend films, the FBTIC neat film has a stronger PL emission and it was quenched in the blend film. In addition, the emission intensity of

the blend film increases in compared with that of Y6 neat film due to the addition of FBTIC, indicating the presence of energy transfer from FBTIC to Y6.

2.3. Film Morphology

Atomic force microscope (AFM) was used to display the surface morphology information of the active layer (Figure S3). Root-mean-square (RMS) roughness of PM6/Y6, PM6/FBTIC and PM6/Y6/FBTIC (1.0/1.0/0.2) blend films are 3.10, 3.82 and 2.93 nm, respectively. The ternary blend film exhibits a more uniform aggregation domains and smoother surface compared to binary blend films.

Grazing-incidence wide-angle X-ray scattering (GIWAXS) were conducted to study the nanoscale morphology of the pure/binary/ternary films. As shown in Figure S4, the pure PM6 film shows obvious (100) lamellar peaks in both in-plane (IP) and out-of-plane (OOP) direction at q_r = 0.295 $Å^{-1}$ (d = 21.3 Å), and q_z = 0.320 $Å^{-1}$ (d = 19.6 Å), consistent with previous reports.[56] The pure Y6 film exhibits preferred face-on orientation, showing a prominent π-π peak at q_z = 1.77 $Å^{-1}$ (d = 3.55 Å), and two peaks at q_r = 0.270 $Å^{-1}$ (d = 23.3 Å) and 0.410 $Å^{-1}$ (d = 15.3 Å), which are considered to originate from lamellar and end group π-π stacking of Y6. The pure FBTIC also presents face-on orientation with the π-π peak at q_z = 1.78 $Å^{-1}$ (d = 3.53 Å) and the (100) lamellar peak at q_r = 0.387 $Å^{-1}$ (d = 16.2 Å). Compared with pure Y6, the crystallinity of pure FBTIC is much weaker, it's likely that the 3D shape of FBTIC impedes its crystalline packing.

In Figure 5, the binary PM6/Y6 blend film remains dominantly face-on oriented with the lamellar peak at q_r = 0.289 $Å^{-1}$ (d = 21.7 Å) and the π-π peak at q_z = 1.75 $Å^{-1}$

(d =3.59 Å). The ternary PM6/Y6/FBTIC (1.0/1.0/0.2) film presents almost the same scattering features as the binary PM6/Y6 film in terms of crystallinity and molecular orientation. Together, it suggests that the 3D staked FBTIC crystalline domains are easy to be disrupted by the second component. Therefore, it's possible that the FBTIC molecules are loosely distributed around the PM6/Y6 domains in the PM6/Y6/FBTIC (1.0/1.0/0.2) ternary system without changing its overall morphology. This is further confirmed by the grazing incidence small-angle X-ray scattering (GISAXS).

GISAXS measurements were further performed to probe nanoscale morphology of binary and ternary blend films. Figure 6 presents the two-dimensional (2D) GISAXS patterns and the corresponding intensity profiles along the in-plane direction. Fitted with the Debye-Anderson-Brumberger (DAB) model and the fractal-like network model,[78, 79] the correlation length (ξ) of intermixing amorphous phase and the average domain size ($2R_g$) of clustered acceptor phases are quantified and summarized in Table S3. The average domain sizes ($2R_g$) for binary PM6/Y6 film and ternary PM6/Y6/FBTIC (1.0/1.0/0.2) film are 18.5 nm and 22.2 nm respectively, which are close to the theoretical exciton length diffusion for efficient charge separation. The similar clustered acceptor sizes indicate the stacking of Y6 are largely reserved. Moreover, the recent research reveals the hierarchical structure in the ternary/quaternary organic solar cell, which is quite similar with the PM6/Y6/FBTIC (1.0/1.0/0.2) ternary system.[80] The PM6/FBTIC smaller domains are likely to be distributed at the PM6/Y6 domains boundary, this hierarchical structure could suppress charge recombination, enhance the charge transport, and therefore improve the V_{OC}.

The amorphous intermixing domain of ternary PM6/Y6/FBTIC (1.0/1.0/0.2) shrink a little from 52.3 nm to 49.4 nm, possibly due to the interference of FBTIC, which could enhance the exciton utilization from amorphous regions.

In conclusion, based on both the GIWAXS and GISAXS results, the introduction of FBTIC has little influence on the film bulk morphology. The PM6/Y6 binary blends largely reserve the original heterojunction framework, the optimized phase separation and domain size. This would be beneficial for the reservation of efficient charge transfer channels which are related to the device FF and J_{SC}.

3. CONCLUSION

To summarize, a series of organic photovoltaic devices were fabricated based on PM6/Y6, PM6/FBTIC binary system and PM6/Y6/FBTIC ternary system. The guest acceptor FBTIC exhibits a great match in both light absorption and LUMO with the host acceptor Y6. Compared with binary devices, the ternary devices effectively enhance the efficiency of exciton dissociation and charge collection due to the cross-linking functionality of star-shaped chemical structure of FBTIC. The best PCE of the devices based on PM6/Y6, PM6/FBTIC and PM6/Y6/FBTIC are 16.0%, 8.84% and 16.7%, respectively. FBTIC is highly compatible with PM6/Y6 system and can increase the V_{OC} considerably without deteriorating the optical properties and thin film morphology. Therefore, it might be a universal third component, which can work with many other high-performance binary systems.

EXPERIMENTAL SECTION

Materials. PM6, Y6 and PNDIT-F3N were purchased from Derthon Optoelectronic

Materials Science Technology Co., LTD and 1-Material Inc., respectively. FBTIC was synthesized according to our reported procedures (ref 15).

Device Fabrication and Characterization. Both conventional and inverted device structures are used in this work. The fabrications of conventional and inverted device were according to ref 77 and 15, respectively, and the*J*–*V* curves and EQE spectra of all encapsulated devices were measured using the apparatus described in ref 52. Both sample preparation and measurements of AFM, GIWAXS and GISAXS were used the same method as reported in ref 15. The more details of device fabrication and characterization, see Supporting Information.

ASSOCIATED CONTENT

Supporting Information. This material is available free of charge via the Internet at http://pubs.acs.org.

SCLC, AFM and GIWAXS; OSC fabrication and characterization; CCDC 1911552 and 2015912 contains the supplementary crystallographic data for this paper. These data can be obtained free of charge from The Cambridge Crystallographic Data Centre via www.ccdc.cam.ac.uk/data_request/cif.

AUTHOR INFORMATION

Corresponding Author

*E-mail: glcai@cuhk.edu.hk (G.C); xinhui.lu@cuhk.edu.hk (X.L.)

Notes

The authors declare no competing financial interest.

ACKNOWLEDGMENT

G.C. and X.L. acknowledge the financial support from UGC/RGC fund (Project No. JLFS/P-102/18) and NSFC/RGC Joint Research Scheme (Grant No. N_CUHK418/17). X.Z. thanks NSFC (51761165023). Z.X. thanks the financial support from NSFC (21733005 and 51761135101). G. L thanks the support from UGC/RGC fund (Project Nos 15218517, C5037-18G).

REFERENCES

(1) Yu, G.; Gao, J.; Hummelen, J. C.; Wudl, F.; Heeger, A. J. Polymer Photovoltaic Cells-Enhanced Efficiencies Via a Network of Internal Donor-Acceptor Heterojunctions. *Science* **1995**, *270*, 1789-1791.

(2) Li, G.; Zhu, R.; Yang, Y. Polymer Solar Cells. *Nat. Photon.* **2012**, *6*, 153-161.

(3) Lu, L.; Zheng, T.; Wu, Q.; Schneider, A. M.; Zhao, D.; Yu, L. Recent Advances in Bulk Heterojunction Polymer Solar Cells. *Chem. Rev.* **2015**, *115*, 12666-12731.

(4) Li, Y. Molecular Design of Photovoltaic Materials for Polymer Solar Cells: Toward Suitable Electronic Energy Levels and Broad Absorption. *Acc. Chem. Res.* **2012**, *45*, 723-733.

(5) Li, M.; Gao, K.; Wan, X.; Zhang, Q.; Kan, B.; Xia, R.; Liu, F.; Yang, X.; Feng, H.; Ni, W.; Wang, Y.; Peng, J.; Zhang, H.; Liang, Z.; Yip, H. L.; Peng, X.; Cao, Y.; Chen, Y. Solution-Processed Organic Tandem Solar Cells with Power Conversion Efficiencies >12%. *Nat. Photon.* **2016**, *11*, 85-90.

(6) Zhao, J.; Li, Y.; Yang, G.; Jiang, K.; Lin, H.; Ade, H.; Ma, W.; Yan, H. Efficient Organic Solar Cells Processed from Hydrocarbon Solvents. *Nat. Energy* **2016**, *1*, 15027.

(7) Zhou, Z. C.; Xu, S. J.; Song, J. N.; Jin, Y. Z.; Yue, Q. H.; Qian, Y. H.; Liu, F.;

Zhang, F. L.; Zhu, X. Z. High-Efficiency Small-Molecule Ternary Solar Cells with a Hierarchical Morphology Enabled by Synergizing Fullerene and Non-Fullerene Acceptors. *Nat. Energy* **2018**, *3*, 952-959.

(8) Lin, Y.; Zhan, X. Designing Efficient Non-Fullerene Acceptors by Tailoring Extended Fused-Rings with Electron-Deficient Groups. *Adv. Energy Mater.* **2015**, *5*, 1501063.

(9) Lin, Y.; Zhan, X. Non-Fullerene Acceptors for Organic Photovoltaics: An Emerging Horizon. *Mater. Horizons* **2014**, *1*, 470-488.

(10) Lin, Y.; Wang, J.; Zhang, Z. G.; Bai, H.; Li, Y.; Zhu, D.; Zhan, X. An Electron Acceptor Challenging Fullerenes for Efficient Polymer Solar Cells. *Adv. Mater.* **2015**, *27*, 1170-1174.

(11) Lin, Y.; He, Q.; Zhao, F.; Huo, L.; Mai, J.; Lu, X.; Su, C. J.; Li, T.; Wang, J.; Zhu, J.; Sun, Y.; Wang, C.; Zhan, X. A Facile Planar Fused-Ring Electron Acceptor for as-Cast Polymer Solar Cells with 8.71% Efficiency. *J. Am. Chem. Soc.* **2016**, *138*, 2973-2976.

(12) Liu, W.; Zhang, J.; Zhou, Z.; Zhang, D.; Zhang, Y.; Xu, S.; Zhu, X. Design of a New Fused-Ring Electron Acceptor with Excellent Compatibility to Wide-Bandgap Polymer Donors for High-Performance Organic Photovoltaics. *Adv. Mater.* **2018**, *30*, 1800403.

(13) Cai, G.; Zhu, J.; Xiao, Y.; Li, M.; Liu, K.; Wang, J.; Wang, W.; Lu, X.; Tang, Z.; Lian, J.; Zeng, P.; Wang, Y.; Zhan, X. Fused Octacyclic Electron Acceptor Isomers for Organic Solar Cells. *J. Mater. Chem. A* **2019**, *7*, 21432-21437.

(14) Geng, R.; Song, X.; Feng, H.; Yu, J.; Zhang, M.; Gasparini, N.; Zhang, Z.; Liu, F.; Baran, D.; Tang, W. Nonfullerene Acceptor for Organic Solar Cells with Chlorination on Dithieno [3, 2-B: 2′, 3′-D] Pyrrol Fused-Ring. *ACS Energy Lett.* **2019**, *4*, 763-770.

(15) Cai, G.; Wang, W.; Zhou, J.; Xiao, Y.; Liu, K.; Xie, Z.; Lu, X.; Lian, J.; Zeng, P.; Wang, Y.; Zhan, X. Comparison of Linear- and Star-Shaped Fused-Ring Electron Acceptors. *ACS Mater. Lett.* **2019**, *1*, 367-374.

(16) Yao, Z.; Liao, X.; Gao, K.; Lin, F.; Xu, X.; Shi, X.; Zuo, L.; Liu, F.; Chen, Y.; Jen, A. K. Dithienopicenocarbazole-Based Acceptors for Efficient Organic Solar Cells with Optoelectronic Response over 1000 Nm and an Extremely Low Energy Loss. *J. Am. Chem. Soc.* **2018**, *140*, 2054-2057.

(17) Wang, J.; Zhang, J.; Xiao, Y.; Xiao, T.; Zhu, R.; Yan, C.; Fu, Y.; Lu, G.; Lu, X.; Marder, S. R.; Zhan, X. Effect of Isomerization on High-Performance Nonfullerene Electron Acceptors. *J. Am. Chem. Soc.* **2018**, *140*, 9140-9147.

(18) Zhu, J.; Ke, Z.; Zhang, Q.; Wang, J.; Dai, S.; Wu, Y.; Xu, Y.; Lin, Y.; Ma, W.; You, W.; Zhan, X. Naphthodithiophene-Based Nonfullerene Acceptor for High-Performance Organic Photovoltaics: Effect of Extended Conjugation. *Adv. Mater.* **2018**, *30*, 1704713.

(19) Liu, G. C.; Jia, J. C.; Zhang, K.; Jia, X. E.; Yin, Q. W.; Zhong, W. K.; Li, L.; Huang, F.; Cao, Y. 15% Efficiency Tandem Organic Solar Cell Based on a Novel Highly Efficient Wide-Bandgap Nonfullerene Acceptor with Low Energy Loss. *Adv. Energy Mater.* **2019**, *9*, 1803657.

(20) Sun, J.; Ma, X.; Zhang, Z.; Yu, J.; Zhou, J.; Yin, X.; Yang, L.; Geng, R.; Zhu, R.;

Zhang, F.; Tang, W. Dithieno[3,2-B:2',3'-D]Pyrrol Fused Nonfullerene Acceptors Enabling over 13% Efficiency for Organic Solar Cells. *Adv. Mater.* **2018**, *30*, 1707150.

(21) Wang, W.; Yan, C.; Lau, T. K.; Wang, J.; Liu, K.; Fan, Y.; Lu, X.; Zhan, X. Fused Hexacyclic Nonfullerene Acceptor with Strong near-Infrared Absorption for Semitransparent Organic Solar Cells with 9.77% Efficiency. *Adv. Mater.* **2017**, *29*, 1701308.

(22) Yuan, J.; Huang, T.; Cheng, P.; Zou, Y.; Zhang, H.; Yang, J. L.; Chang, S. Y.; Zhang, Z.; Huang, W.; Wang, R.; Meng, D.; Gao, F.; Yang, Y. Enabling Low Voltage Losses and High Photocurrent in Fullerene-Free Organic Photovoltaics. *Nat. Commun.* **2019**, *10*, 570.

(23) Li, T.; Dai, S.; Ke, Z.; Yang, L.; Wang, J.; Yan, C.; Ma, W.; Zhan, X. Fused Tris(Thienothiophene)-Based Electron Acceptor with Strong near-Infrared Absorption for High-Performance as-Cast Solar Cells. *Adv. Mater.* **2018**, *30*, 1705969.

(24) Wang, J.; Wang, W.; Wang, X.; Wu, Y.; Zhang, Q.; Yan, C.; Ma, W.; You, W.; Zhan, X. Enhancing Performance of Nonfullerene Acceptors Via Side-Chain Conjugation Strategy. *Adv. Mater.* **2017**, *29*, 1702125.

(25) Kan, B.; Feng, H.; Wan, X.; Liu, F.; Ke, X.; Wang, Y.; Wang, Y.; Zhang, H.; Li, C.; Hou, J.; Chen, Y. Small-Molecule Acceptor Based on the Heptacyclic Benzodi(Cyclopentadithiophene) Unit for Highly Efficient Nonfullerene Organic Solar Cells. *J. Am. Chem. Soc.* **2017**, *139*, 4929-4934.

(26) Cai, G.; Xue, P.; Chen, Z.; Li, T.; Liu, K.; Ma, W.; Lian, J.; Zeng, P.; Wang, Y.; Han, R. P. S.; Zhan, X. High-Performance Mid-Bandgap Fused-Pyrene Electron

Acceptor. *Chem. Mater.* **2019**, *31*, 6484-6490.

(27) Kan, B.; Feng, H.; Wan, X.; Liu, F.; Ke, X.; Wang, Y.; Wang, Y.; Zhang, H.; Li, C.; Hou, J.; Chen, Y. Small-Molecule Acceptor Based on the Heptacyclic Benzodi (Cyclopentadithiophene) Unit for Highly Efficient Nonfullerene Organic Solar Cells. *J. Am. Chem. Soc.* **2017**, *139*, 4929-4934.

(28) Cai, G.; Xiao, Y.; Li, M.; Rech, J. J.; Wang, J.; Liu, K.; Lu, X.; Tang, Z.; Lian, J.; Zeng, P.; Wang, Y.; You, W.; Zhan, X. Effects of Linking Units on Fused-Ring Electron Acceptor Dimers. *J. Mater. Chem. A* **2020**, *8*, 13735-13741.

(29) Jia, B.; Wang, J.; Wu, Y.; Zhang, M.; Jiang, Y.; Tang, Z.; Russell, T. P.; Zhan, X. Enhancing the Performance of a Fused-Ring Electron Acceptor by Unidirectional Extension. *J. Am. Chem. Soc.* **2019**, *141*, 19023-19031.

(30) Yang, J.; Chen, F.; Hu, J.; Geng, Y.; Zeng, Q.; Tang, A.; Wang, X.; Zhou, E. Planar Benzofuran inside-Fused Perylenediimide Dimers for High Voc Fullerene-Free Organic Solar Cells. *ACS Appl. Mater. Interfaces* **2019**, *11*, 4203-4210.

(31) Wang, Z.; Xiao, M.; Liu, X.; He, B.; Yang, X.; Li, Y.; Peng, J.; Huang, F.; Cao, Y. Naphthalenediimide-Based N-Type Polymer Acceptors with Pendant Twisted Perylenediimide Units for All-Polymer Solar Cells. *Polymer* **2018**, *158*, 183-189.

(32) Shiau, S.-Y.; Chang, C.-H.; Chen, W.-J.; Wang, H.-J.; Jeng, R.-J.; Lee, R.-H. Star-Shaped Organic Semiconductors with Planar Triazine Core and Diketopyrrolopyrrole Branches for Solution-Processed Small-Molecule Organic Solar Cells. *Dyes Pigments* **2015**, *115*, 35-49.

(33) Zhang, M.; Gao, W.; Zhang, F.; Mi, Y.; Wang, W.; An, Q.; Wang, J.; Ma, X.; Miao,

J.; Hu, Z. Efficient Ternary Non-Fullerene Polymer Solar Cells with Pce of 11.92% and Ff of 76.5%. *Energy Environ. Sci.* **2018**, *11*, 841-849.

(34) Li, S.; Ye, L.; Zhao, W.; Zhang, S.; Mukherjee, S.; Ade, H.; Hou, J. Energy-Level Modulation of Small-Molecule Electron Acceptors to Achieve over 12% Efficiency in Polymer Solar Cells. *Adv. Mater.* **2016**, *28*, 9423-9429.

(35) Zhao, F.; Dai, S.; Wu, Y.; Zhang, Q.; Wang, J.; Jiang, L.; Ling, Q.; Wei, Z.; Ma, W.; You, W.; Wang, C.; Zhan, X. Single-Junction Binary-Blend Nonfullerene Polymer Solar Cells with 12.1% Efficiency. *Adv. Mater.* **2017**, *29*, 1700144.

(36) Liu, T.; Luo, Z. H.; Fan, Q. P.; Zhang, G. Y.; Zhang, L.; Gao, W.; Guo, X.; Ma, W.; Zhang, M. J.; Yang, C. L.; Li, Y. F.; Yan, H. Use of Two Structurally Similar Small Molecular Acceptors Enabling Ternary Organic Solar Cells with High Efficiencies and Fill Factors. *Energy Environ. Sci.* **2018**, *11*, 3275-3282.

(37) Aldrich, T. J.; Matta, M.; Zhu, W.; Swick, S. M.; Stern, C. L.; Schatz, G. C.; Facchetti, A.; Melkonyan, F. S.; Marks, T. J. Fluorination Effects on Indacenodithienothiophene Acceptor Packing and Electronic Structure, End-Group Redistribution, and Solar Cell Photovoltaic Response. *J. Am. Chem. Soc.* **2019**, *141*, 3274-3287.

(38) Wang, Y.; Zhang, Y.; Qiu, N.; Feng, H.; Gao, H.; Kan, B.; Ma, Y.; Li, C.; Wan, X.; Chen, Y. A Halogenation Strategy for over 12% Efficiency Nonfullerene Organic Solar Cells. *Adv. Energy Mater.* **2018**, *8*, 1702870.

(39) Dai, S.; Zhao, F.; Zhang, Q.; Lau, T. K.; Li, T.; Liu, K.; Ling, Q.; Wang, C.; Lu, X.; You, W.; Zhan, X. Fused Nonacyclic Electron Acceptors for Efficient Polymer

Solar Cells. *J. Am. Chem. Soc.* **2017**, *139*, 1336-1343.

(40) Luo, Z.; Bin, H.; Liu, T.; Zhang, Z. G.; Yang, Y.; Zhong, C.; Qiu, B.; Li, G.; Gao, W.; Xie, D.; Wu, K.; Sun, Y.; Liu, F.; Li, Y.; Yang, C. Fine-Tuning of Molecular Packing and Energy Level through Methyl Substitution Enabling Excellent Small Molecule Acceptors for Nonfullerene Polymer Solar Cells with Efficiency up to 12.54%. *Adv. Mater.* **2018**, *30*, 1706124.

(41) Liu, T.; Zhang, Y.; Shao, Y.; Ma, R.; Luo, Z.; Xiao, Y.; Yang, T.; Lu, X.; Yuan, Z.; Yan, H.; Chen, Y.; Li, Y. Asymmetric Acceptors with Fluorine and Chlorine Substitution for Organic Solar Cells toward 16.83% Efficiency. *Adv. Funct. Mater.* **2020**, *30*, 2000456.

(42) Lai, H.; Zhao, Q.; Chen, Z.; Chen, H.; Chao, P.; Zhu, Y.; Lang, Y.; Zhen, N.; Mo, D.; Zhang, Y.; He, F. Trifluoromethylation Enables a 3d Interpenetrated Low-Band-Gap Acceptor for Efficient Organic Solar Cells. *Joule* **2020**, *4*, 688-700.

(43) Afzal, Z.; Hussain, R.; Khan, M. U.; Khalid, M.; Iqbal, J.; Alvi, M. U.; Adnan, M.; Ahmed, M.; Mehboob, M. Y.; Hussain, M.; Tariq, C. J. Designing Indenothiophene-Based Acceptor Materials with Efficient Photovoltaic Parameters for Fullerene-Free Organic Solar Cells. *J. Mol. Model.* **2020**, *26*, 137.

(44) Shehzad, R. A.; Iqbal, J.; Khan, M. U.; Hussain, R.; Javed, H. M. A.; Rehman, A. u.; Alvi, M. U.; Khalid, M. Designing of Benzothiazole Based Non-Fullerene Acceptor (NFA) Molecules for Highly Efficient Organic Solar Cells. *Comput. Theor. Chem.* **2020**, *1181*, 112833.

(45) Fei, Z.; Eisner, F. D.; Jiao, X.; Azzouzi, M.; Rohr, J. A.; Han, Y.; Shahid, M.;

Chesman, A. S. R.; Easton, C. D.; McNeill, C. R.; Anthopoulos, T. D.; Nelson, J.; Heeney, M. An Alkylated Indacenodithieno[3,2-B]Thiophene-Based Nonfullerene Acceptor with High Crystallinity Exhibiting Single Junction Solar Cell Efficiencies Greater Than 13% with Low Voltage Losses. *Adv. Mater.* **2018**, *30*, 1705209.

(46) Lin, Y.; Zhao, F.; He, Q.; Huo, L.; Wu, Y.; Parker, T. C.; Ma, W.; Sun, Y.; Wang, C.; Zhu, D.; Heeger, A. J.; Marder, S. R.; Zhan, X. High-Performance Electron Acceptor with Thienyl Side Chains for Organic Photovoltaics. *J. Am. Chem. Soc.* **2016**, *138*, 4955-4961.

(47) Yang, Y.; Zhang, Z. G.; Bin, H.; Chen, S.; Gao, L.; Xue, L.; Yang, C.; Li, Y. Side-Chain Isomerization on an N-Type Organic Semiconductor Itic Acceptor Makes 11.77% High Efficiency Polymer Solar Cells. *J. Am. Chem. Soc.* **2016**, *138*, 15011-15018.

(48) Cheng, P.; Wang, J.; Zhang, Q.; Huang, W.; Zhu, J.; Wang, R.; Chang, S. Y.; Sun, P.; Meng, L.; Zhao, H.; Cheng, H. W.; Huang, T.; Liu, Y.; Wang, C.; Zhu, C.; You, W.; Zhan, X.; Yang, Y. Unique Energy Alignments of a Ternary Material System toward High-Performance Organic Photovoltaics. *Adv. Mater.* **2018**, *30*, 1801501.

(49) Liu, T.; Gao, W.; Wang, Y.; Yang, T.; Ma, R.; Zhang, G.; Zhong, C.; Ma, W.; Yan, H.; Yang, C. Unconjugated Side-Chain Engineering Enables Small Molecular Acceptors for Highly Efficient Non-Fullerene Organic Solar Cells: Insights into the Fine-Tuning of Acceptor Properties and Micromorphology. *Adv. Funct. Mater.* **2019**, *29*, 1902155.

(50) Dai, S.; Zhou, J.; Chandrabose, S.; Shi, Y.; Han, G.; Chen, K.; Xin, J.; Liu, K.; Chen, Z.; Xie, Z.; Ma, W.; Yi, Y.; Jiang, L.; Hodgkiss, J. M.; Zhan, X. High-

Performance Fluorinated Fused-Ring Electron Acceptor with 3d Stacking and Exciton/Charge Transport. *Adv. Mater.* **2020**, *32*, 2000645.

(51) Ma, R.; Liu, T.; Luo, Z.; Guo, Q.; Xiao, Y.; Chen, Y.; Li, X.; Luo, S.; Lu, X.; Zhang, M.; Li, Y.; Yan, H. Improving Open-Circuit Voltage by a Chlorinated Polymer Donor Endows Binary Organic Solar Cells Efficiencies over 17%. *Sci. China Chem.* **2020**, *63*, 325-330.

(52) Liu, T.; Ma, R.; Luo, Z.; Guo, Y.; Zhang, G.; Xiao, Y.; Yang, T.; Chen, Y.; Li, G.; Yi, Y.; Lu, X.; Yan, H.; Tang, B. Concurrent Improvement in Jsc and Voc in High-Efficiency Ternary Organic Solar Cells Enabled by a Red-Absorbing Small-Molecule Acceptor with a High Lumo Level. *Energy Environ. Sci.* **2020**, *13*, 2115-2123.

(53) Luo, Z. H.; Ma, R. J.; Liu, T.; Yu, J. W.; Xiao, Y. Q.; Sun, R.; Xie, G. S.; Yuan, J.; Chen, Y. Z.; Chen, K.; Chai, G. D.; Sun, H. L.; Min, J.; Zhang, J.; Zou, Y. P.; Yang, C. L.; Lu, X. H.; Gao, F.; Yan, H. Fine-Tuning Energy Levels Via Asymmetric End Groups Enables Polymer Solar Cells with Efficiencies over 17%. *Joule* **2020**, *4*, 1236-1247.

(54) Cui, Y.; Yao, H.; Zhang, J.; Xian, K.; Zhang, T.; Hong, L.; Wang, Y.; Xu, Y.; Ma, K.; An, C.; He, C.; Wei, Z.; Gao, F.; Hou, J. Single-Junction Organic Photovoltaic Cells with Approaching 18% Efficiency. *Adv. Mater.* **2020**, 1908205.

(55) Meng, L.; Zhang, Y.; Wan, X.; Li, C.; Zhang, X.; Wang, Y.; Ke, X.; Xiao, Z.; Ding, L.; Xia, R.; Yip, H. L.; Cao, Y.; Chen, Y. Organic and Solution-Processed Tandem Solar Cells with 17.3% Efficiency. *Science* **2018**, *361*, 1094-1098.

(56) Yuan, J.; Zhang, Y.; Zhou, L.; Zhang, G.; Yip, H.-L.; Lau, T.-K.; Lu, X.; Zhu, C.;

Peng, H.; Johnson, P. A.; Leclerc, M.; Cao, Y.; Ulanski, J.; Li, Y.; Zou, Y. Single-Junction Organic Solar Cell with over 15% Efficiency Using Fused-Ring Acceptor with Electron-Deficient Core. *Joule* **2019**, *3*, 1140-1151.

(57) Zhu, L.; Zhang, M.; Zhou, G. Q.; Hao, T. Y.; Xu, J. Q.; Wang, J.; Qiu, C. Q.; Prine, N.; Ali, J.; Feng, W.; Gu, X. D.; Ma, Z. F.; Tang, Z.; Zhu, H. M.; Ying, L.; Zhang, Y. M.; Liu, F. Efficient Organic Solar Cell with 16.88% Efficiency Enabled by Refined Acceptor Crystallization and Morphology with Improved Charge Transfer and Transport Properties. *Adv. Energy Mater.* **2020**, *10*, 1904234.

(58) Thompson, B. C.; Kim, Y.-G.; Reynolds, J. R. Spectral Broadening in Meh-Ppv:Pcbm-Based Photovoltaic Devices Via Blending with a Narrow Band Gap Cyanovinylene−Dioxythiophene Polymer. *Macromolecules* **2005**, *38*, 5359-5362.

(59) Zhang, Y.; Liu, D.; Lau, T. K.; Zhan, L.; Shen, D.; Fong, P. W. K.; Yan, C.; Zhang, S.; Lu, X.; Lee, C. S.; Hou, J.; Chen, H.; Li, G. A Novel Wide-Bandgap Polymer with Deep Ionization Potential Enables Exceeding 16% Efficiency in Ternary Nonfullerene Polymer Solar Cells. *Adv. Funct. Mater.* **2020**, *30*, 1910466.

(60) Li, D.; Zhu, L.; Liu, X.; Xiao, W.; Yang, J.; Ma, R.; Ding, L.; Liu, F.; Duan, C.; Fahlman, M.; Bao, Q. Enhanced and Balanced Charge Transport Boosting Ternary Solar Cells over 17% Efficiency. *Adv. Mater.* **2020**, 2002344.

(61) Yan, C.; Tang, H.; Ma, R.; Zhang, M.; Liu, T.; Lv, J.; Huang, J.; Yang, Y.; Xu, T.; Kan, Z.; Yan, H.; Liu, F.; Lu, S.; Li, G. Synergy of Liquid-Crystalline Small-Molecule and Polymeric Donors Delivers Uncommon Morphology Evolution and 16.6% Efficiency Organic Photovoltaics. *Adv. Sci.* **2020**, *7*, 2000149.

(62) Yu, R.; Yao, H.; Cui, Y.; Hong, L.; He, C.; Hou, J. Improved Charge Transport and Reduced Nonradiative Energy Loss Enable over 16% Efficiency in Ternary Polymer Solar Cells. *Adv. Mater.* **2019**, *31*, 1902302.

(63) Yan, T.; Song, W.; Huang, J.; Peng, R.; Huang, L.; Ge, Z. 16.67% Rigid and 14.06% Flexible Organic Solar Cells Enabled by Ternary Heterojunction Strategy. *Adv. Mater.* **2019**, *31*, 1902210.

(64) Yan, C.; Liu, T.; Chen, Y.; Ma, R.; Tang, H.; Li, G.; Li, T.; Xiao, Y.; Yang, T.; Lu, X.; Zhan, X.; Yan, H.; Li, G.; Tang, B. Itc-2cl: A Versatile Middle-Bandgap Nonfullerene Acceptor for High-Efficiency Panchromatic Ternary Organic Solar Cells. *Sol. RRL* **2019**, *4*, 1900377.

(65) Gasparini, N.; Paleti, H. K.; Bertrandie, J.; Cai, G. L.; Zhang, G. C.; Wadsworth, A.; Lu, X. H.; Yip, H. L.; McCulloch, I.; Baran, D. Exploiting Ternary Blends for Improved Photostability in High-Efficiency Organic Solar Cells. *ACS Energy Lett.* **2020**, *5*, 1371-1379.

(66) Song, J.; Li, C.; Zhu, L.; Guo, J.; Xu, J.; Zhang, X.; Weng, K.; Zhang, K.; Min, J.; Hao, X.; Zhang, Y.; Liu, F.; Sun, Y. Ternary Organic Solar Cells with Efficiency >16.5% Based on Two Compatible Nonfullerene Acceptors. *Adv. Mater.* **2019**, *31*, 1905645.

(67) Li, K.; Wu, Y.; Tang, Y.; Pan, M. A.; Ma, W.; Fu, H.; Zhan, C.; Yao, J. Ternary Blended Fullerene-Free Polymer Solar Cells with 16.5% Efficiency Enabled with a Higher-Lumo-Level Acceptor to Improve Film Morphology. *Adv. Energy Mater.* **2019**, *9*, 1901728.

(68) Ma, X.; Wang, J.; Gao, J.; Hu, Z.; Xu, C.; Zhang, X.; Zhang, F. Achieving 17.4%

Efficiency of Ternary Organic Photovoltaics with Two Well-Compatible Nonfullerene Acceptors for Minimizing Energy Loss. *Adv. Energy Mater.* **2020**, 2001404.

(69) Yin, H.; Zhang, C.; Hu, H.; Karuthedath, S.; Gao, Y.; Tang, H.; Yan, C.; Cui, L.; Fong, P. W. K.; Zhang, Z.; Gao, Y.; Yang, J.; Xiao, Z.; Ding, L.; Laquai, F.; So, S. K.; Li, G. Highly Crystalline near-Infrared Acceptor Enabling Simultaneous Efficiency and Photostability Boosting in High-Performance Ternary Organic Solar Cells. *ACS Appl. Mater. Interfaces* **2019**, *11*, 48095-48102.

(70) Liu, T.; Luo, Z.; Chen, Y.; Yang, T.; Xiao, Y.; Zhang, G.; Ma, R.; Lu, X.; Zhan, C.; Zhang, M.; Yang, C.; Li, Y.; Yao, J.; Yan, H. A Nonfullerene Acceptor with a 1000 Nm Absorption Edge Enables Ternary Organic Solar Cells with Improved Optical and Morphological Properties and Efficiencies over 15%. *Energy Environ. Sci.* **2019**, *12*, 2529-2536.

(71) Ma, X.; Luo, M.; Gao, W.; Yuan, J.; An, Q.; Zhang, M.; Hu, Z.; Gao, J.; Wang, J.; Zou, Y.; Yang, C.; Zhang, F. Achieving 14.11% Efficiency of Ternary Polymer Solar Cells by Simultaneously Optimizing Photon Harvesting and Exciton Distribution. *Journal of Materials Chemistry A* **2019**, *7*, 7843-7851.

(72) Ma, X. L.; Gao, W.; Yu, J. S.; An, Q. S.; Zhang, M.; Hu, Z. H.; Wang, J. X.; Tang, W. H.; Yang, C. L.; Zhang, F. J. Ternary Nonfullerene Polymer Solar Cells with Efficiency > 13.7% by Integrating the Advantages of the Materials and Two Binary Cells. *Energy Environ. Sci.* **2018**, *11*, 2134-2141.

(73) Zhang, G.; Chen, X. K.; Xiao, J.; Chow, P. C. Y.; Ren, M.; Kupgan, G.; Jiao, X.; Chan, C. C. S.; Du, X.; Xia, R.; Chen, Z.; Yuan, J.; Zhang, Y.; Zhang, S.; Liu, Y.; Zou,

Y.; Yan, H.; Wong, K. S.; Coropceanu, V.; Li, N.; Brabec, C. J.; Bredas, J. L.; Yip, H. L.; Cao, Y. Delocalization of Exciton and Electron Wavefunction in Non-Fullerene Acceptor Molecules Enables Efficient Organic Solar Cells. *Nat. Commun.* **2020**, *11*, 3943.

(74) Zhang, Y.; Shi, L.; Yang, T.; Liu, T.; Xiao, Y.; Lu, X.; Yan, H.; Yuan, Z.; Chen, Y.; Li, Y. Introducing an Identical Benzodithiophene Donor Unit for Polymer Donors and Small-Molecule Acceptors to Unveil the Relationship between the Molecular Structure and Photovoltaic Performance of Non-Fullerene Organic Solar Cells. *J. Mater. Chem. A* **2019**, *7*, 26351-26357.

(75) Zhang, Y.; Cho, Y.; Lee, J.; Oh, J.; Kang, S.-H.; Lee, S. M.; Lee, B.; Zhong, L.; Huang, B.; Lee, S.; Lee, J.-W.; Kim, B. J.; Li, Y.; Yang, C. Volatilizable and Cost-Effective Quinone-Based Solid Additives for Improving Photovoltaic Performance and Morphological Stability in Non-Fullerene Polymer Solar Cells. *J. Mater. Chem. A* **2020**, *8*, 13049-13058.

(76) Malliaras, G. G.; Salem, J. R.; Brock, P. J.; Scott, C. Electrical Characteristics and Efficiency of Single-Layer Organic Light-Emitting Diodes. *Phys. Rev. B* **1998**, *58*, 13411-13414.

(77) Ma, R.; Liu, T.; Luo, Z.; Gao, K.; Chen, K.; Zhang, G.; Gao, W.; Xiao, Y.; Lau, T.-K.; Fan, Q.; Chen, Y.; Ma, L.-K.; Sun, H.; Cai, G.; Yang, T.; Lu, X.; Wang, E.; Yang, C.; Jen, A. K. Y.; Yan, H. Adding a Third Component with Reduced Miscibility and Higher Lumo Level Enables Efficient Ternary Organic Solar Cells. *ACS Energy Lett.* **2020**, *5*, 2711-2720.

(78) Mai, J.; Xiao, Y.; Zhou, G.; Wang, J.; Zhu, J.; Zhao, N.; Zhan, X.; Lu, X. Hidden Structure Ordering Along Backbone of Fused-Ring Electron Acceptors Enhanced by Ternary Bulk Heterojunction. *Adv. Mater.* **2018**, *30*, 1802888.

(79) Mai, J.; Lau, T.-K.; Li, J.; Peng, S.-H.; Hsu, C.-S.; Jeng, U. S.; Zeng, J.; Zhao, N.; Xiao, X.; Lu, X. Understanding Morphology Compatibility for High-Performance Ternary Organic Solar Cells. *Chem. Mater.* **2016**, *28*, 6186-6195.

(80) Arunagiri, L.; Peng, Z.; Zou, X.; Yu, H.; Zhang, G.; Wang, Z.; Lin Lai, J. Y.; Zhang, J.; Zheng, Y.; Cui, C.; Huang, F.; Zou, Y.; Wong, K. S.; Chow, P. C. Y.; Ade, H.; Yan, H. Selective Hole and Electron Transport in Efficient Quaternary Blend Organic Solar Cells. *Joule* **2020**. DOI: 10.1016/j.joule.2020.06.014.

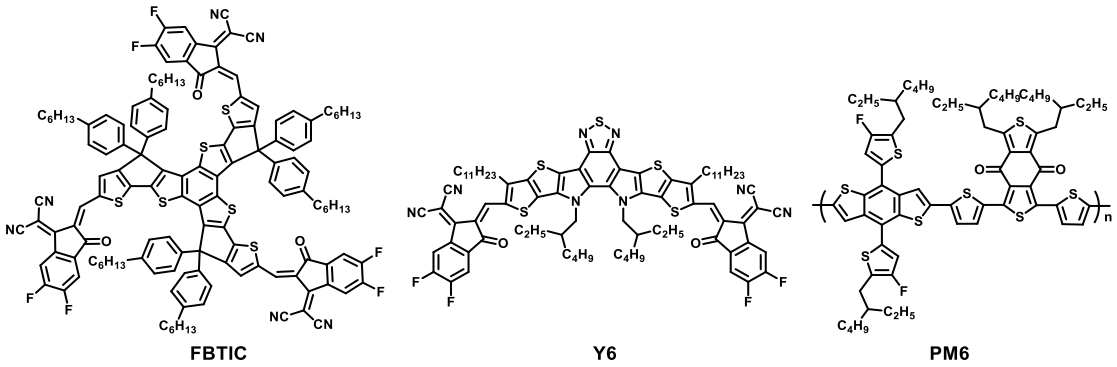

Figure 1. Chemical structures of FBTIC, Y6 and PM6.

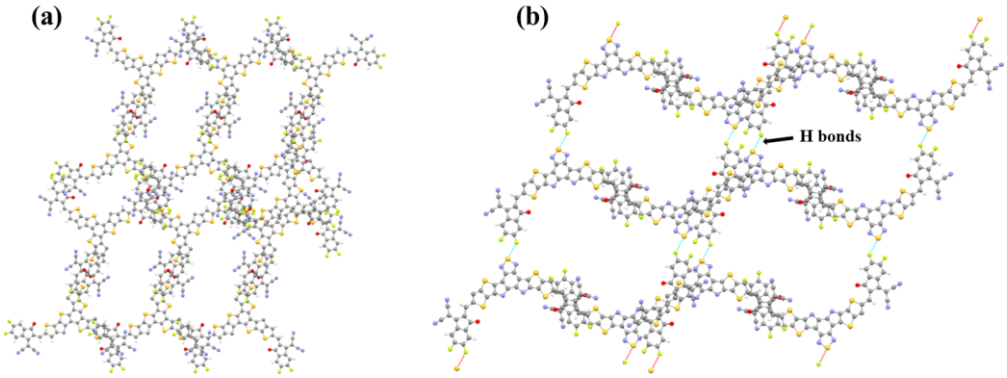

Figure 2. Molecular stacking patterns of (a) FBTIC and (b) Y6 in the single crystal structures.

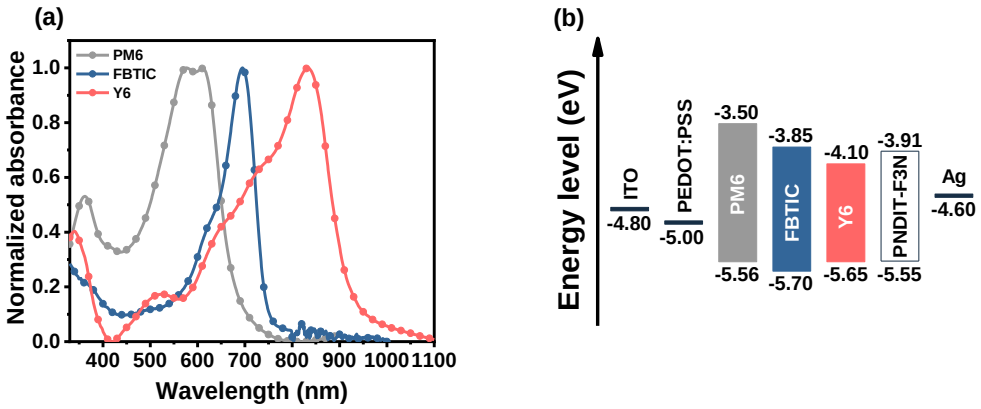

Figure 3. (a) UV-vis absorption spectra of PM6, FBTIC and Y6 in thin films. (b) Energy level alignment of materials.

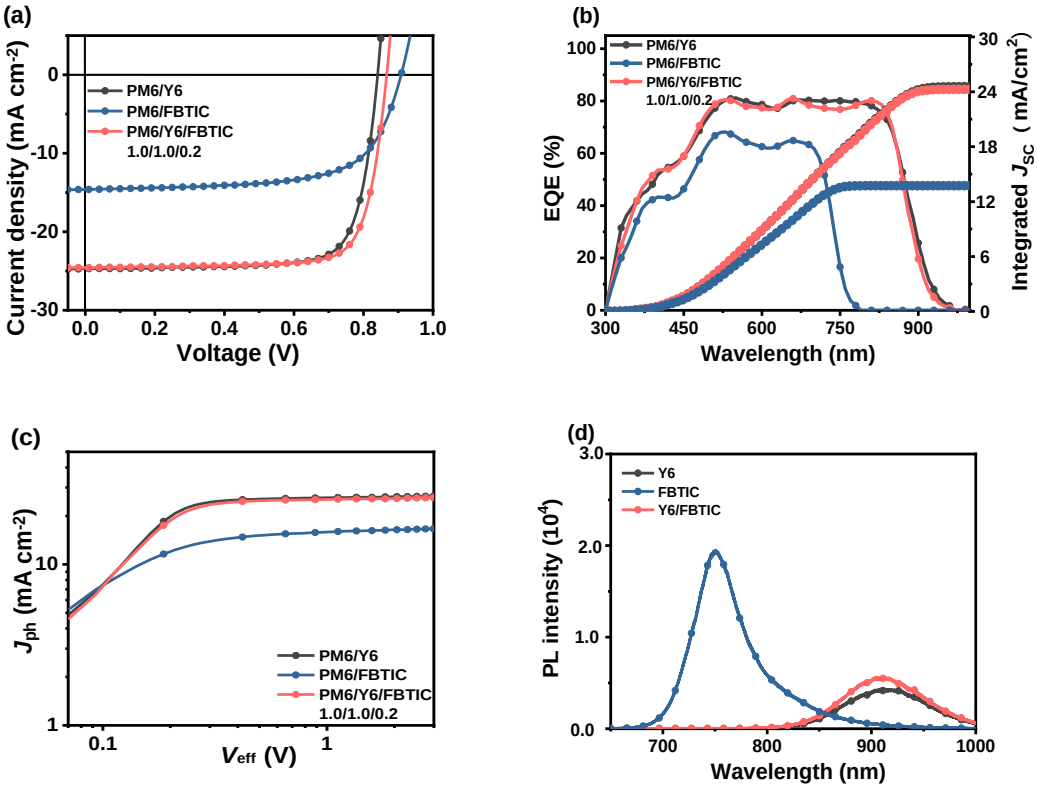

Figure 4. (a) *J*–*V* characteristics and (b) EQE spectra of the optimized OSCs; (c) J_{ph} versus V_{eff} characteristics and (d) PL spectra of acceptor films (excited at 532 nm).

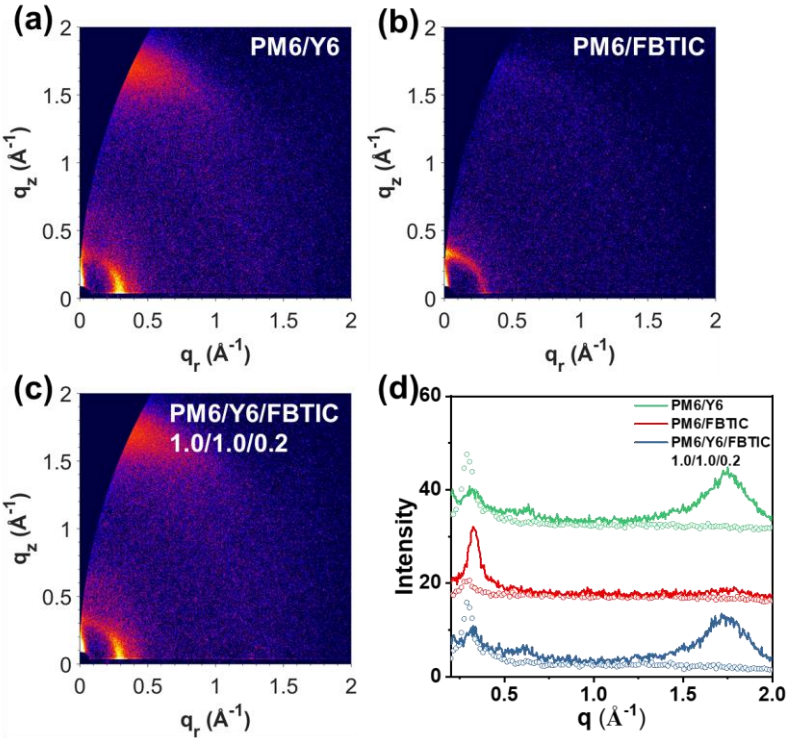

Figure 5. GIWAXS patterns of (a) PM6/Y6, (b) PM6/FBTIC and (c) PM6/Y6/FBTIC blend films, and (d) the corresponding intensity profiles along the in-plane (dashed line) and out-of-plane (solid line) directions.

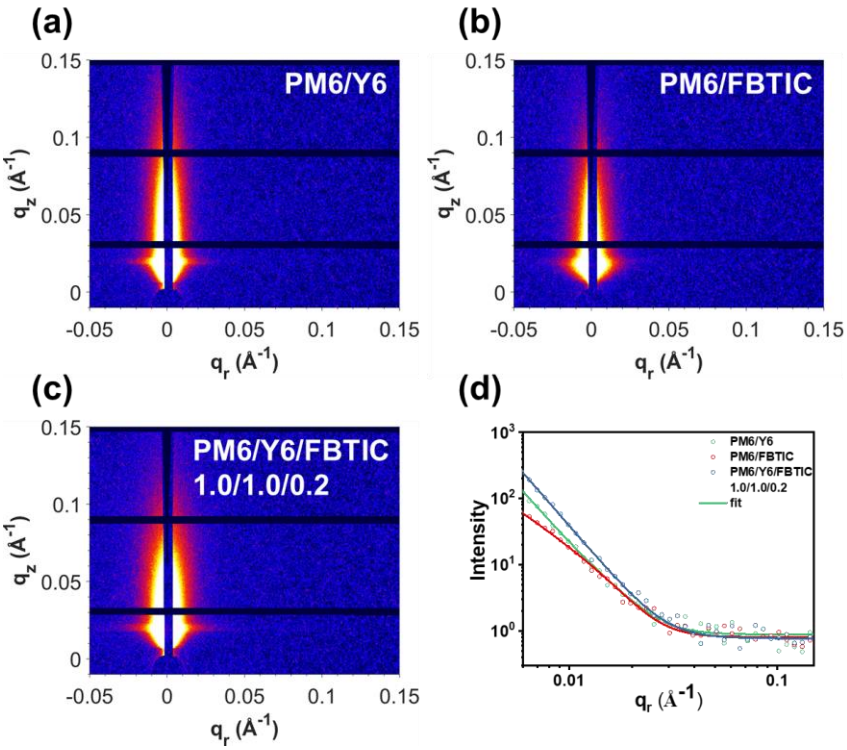

Figure 6. (a, b and c) 2D GISAXS patterns of the blends. (d) The corresponding GISAXS profiles and best fittings along the in-plane.

Table 1. Performance of the optimized OSCs based on PM6/Acceptors with different D/A(s) ratio.

D/A(s)	V_{OC} [a] (V)	J_{SC} [a] (mA cm^{-2})	FF [a] (%)	PCE [a] (%)	calculated J_{SC} (mA cm^2)
PM6/Y6 (1.0/1.2)	0.841 (0.843±0.006)	24.7 (24.6±0.1)	77.3 (76.9±0.9)	16.0 (15.9±0.1)	24.5
PM6/FBTIC (1.0/1.2)	0.908 (0.907±0.009)	14.6 (14.4±0.3)	66.6 (66.3±0.5)	8.84 (8.65±0.23)	13.9
PM6/Y6/FBTIC (1.0/1.1/0.1)	0.850 (0.851±0.005)	25.1 (25.0±0.2)	77.6 (77.0±0.7)	16.5 (16.3±0.2)	24.7
PM6/Y6/FBTIC (1.0/1.0/0.2)	0.866 (0.862±0.009)	24.6 (24.5±0.2)	77.9 (77.5±0.6)	16.7 (16.4±0.2)	24.3
PM6/Y6/FBTIC (1.0/1.0/0.2) [b]	0.856 (0.850±0.006)	23.8 (24.0±0.2)	71.3 (70.0±1.2)	14.5 (14.2±0.2)	23.9
PM6/Y6/FBTIC (1.0/0.9/0.3)	0.874 (0.869±0.006)	23.6 (23.5±0.1)	76.4 (76.1±0.5)	15.8 (15.6±0.1)	23.5

[a] Average values (in parenthesis) are obtained from 20 devices. [b] The OSCs were fabricated with an inverted structure: indium tin oxide (ITO) glass/ZnO/active layer/MoO_3/Ag.

TABLE of CONTENTS